Improving light harvesting in polymer photodetector devices through nanoindented metal mask films

A. G. Macedo,[1,2] F. Zanetti,[1] A. Mikowski,[1] J. C. Hummelen,[3] C. M. Lepienski,[1] M. G. E. da Luz,[1,a)] and L. S. Roman[1,b)]
[1]*Departamento de Física, Universidade Federal do Paraná, 81531-990 Curitiba-PR, Brazil*
[2]*Departamento de Física, Universidade de Aveiro, 3810-193 Aveiro, Portugal*
[3]*Zernike Institute for Advanced Materials, University of Groningen, Nijenborgh 4, NL-9747AG Groningen, The Netherlands*

(Received 22 April 2008; accepted 11 July 2008; published online 13 August 2008)

To enhance light harvesting in organic photovoltaic devices, we propose the incorporation of a metal (aluminum) mask film in the system's usual layout. We fabricate devices in a sandwich geometry, where the mask (nanoindented with a periodic array of holes of sizes d and spacing s) is added between the transparent electrode and the active layer formed by a blend of the semiconducting polymer P3HT and substituted fullerene. Its function is to promote trapping of the incident light into the device's cavity (the region corresponding to the active layer). For d, we set a value that allows light diffraction through the holes in the relevant absorption range of the polymer. To optimize the mask structure, we consider a very simple model to determine the s leading to trapped fields that are relatively intense and homogeneous within the device. From measurements of the action spectra, we show that, indeed, such architecture can considerably improve the resulting photocurrent efficiencies—one order of magnitude in the best situation studied. © *2008 American Institute of Physics*. [DOI: 10.1063/1.2968250]

I. INTRODUCTION

Conjugated polymers generally present high absorption, an important feature for their use as an active layer in photovoltaic devices.[1,2] However, the mechanisms[3] involved in the photocurrent creation (the necessity of the formed exciton to undergo charge dissociation instead of dissipative recombination) and the system transport properties (e.g., low mobility of the charges) set limits for the device thickness. Such restriction causes a reduction in the amount of absorbed light, consequently decreasing the photocurrent.

There are different ways to overcome the problem. One idea is to increase the excitons' dissociation rates by increasing the number of donorlike or acceptorlike interfaces through building of devices with multiple or highly folded interfaces.[4,5] Another possibility is to improve the light harvesting itself. For that, some methods have been investigated. Two very explored approaches are (i) to obtain higher efficiencies in light absorption by directly "engineering" the active layer, e.g., through doping,[6] molecular blends,[7] among others, and (ii) to enhance the quantity of light in the system active region by incorporating optical elements in the device's architecture as, for instance, photonic crystals,[8] microlenses,[9] scattering layers,[10] dielectric mirrors,[11] gratings,[12] and folding substrates,[13] to cite just a few.

Along line (ii) discussed above, a particularly good procedure for the case of thin cell geometries is to make the incident photons follow a multiple passes "trajectory" within the light absorbing organic layer.[14] Usually, the setups devised for so[14–16] are based on some light trapping structure.

Here we show that by adding a very simple structure—a metal mask—to the traditional layout of an organic photovoltaic device, we can achieve the mentioned multiple passes in the polymer layer with a consequent growth of the photocurrent. The metal mask is just an aluminum film with a regular array of holes (building up from a nanoindenter), disposed between the transparent electrode [fluorine doped tin oxide (FTO)] and the polymer layer.

The present work is organized as the following. We first show a series of experimental studies in order to determine the ideal indentation charges as function of the metal mask thickness leading to holes with the appropriate size of about 500 nm for our applications (the wavelength range that the polymer in the devices absorbs is 450–700 nm). Then, we use a straightforward model to calculate the optimal distances between the holes to get a uniform distribution of light in the system's "cavity" (the whole region between the metal mask and the top electrode), which, in the final device, should correspond to the space filled with the polymer. Finally, we fabricate different samples and perform measurements of J as a function of the incident light λ. We find that for particular values of the mask relevant parameters (predicted by the simulations), indeed, the resulting photocurrents are much higher than those observed for similar devices but with no masks.

II. EXPERIMENTAL

The devices were fabricated in a sandwich geometry using FTO (Flexitec Ltd.) and aluminum as electrodes. The active layer was a blend of a donor, the semiconducting polymer poly(3-hexylthiophene) (P3HT) from Aldrich (5 mg/ml), and an acceptor, the molecule [6,6]-phenyl-C_{61}-butyric acid

a)Electronic mail: luz@fisica.ufpr.br.
b)Electronic mail: lsroman@fisica.ufpr.br.

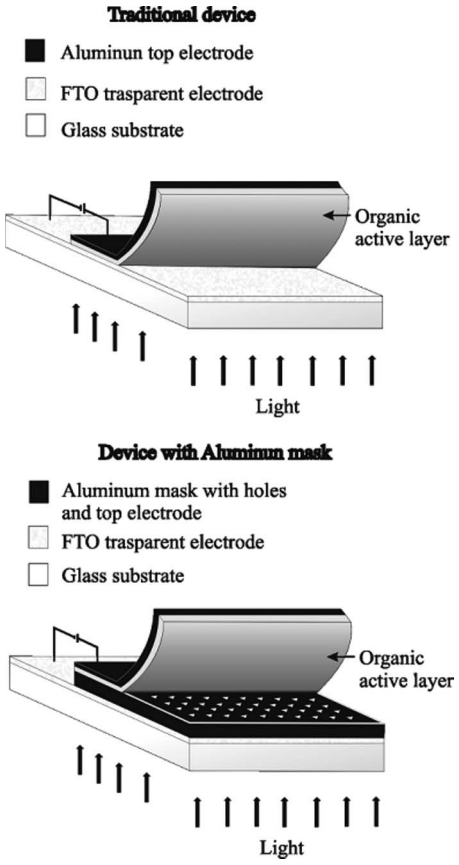

FIG. 1. Schematic representation of the photovoltaic devices sandwich structure: the traditional setup, where the active layer [P3HT:PCBM (1:1)] is between the FTO and aluminum electrodes, and the version with the indented mask between the active layer and the FTO.

methyl ester (PCBM),[17] both dissolved in chloroform with a ratio of 1:1. The solution was cast onto either patterned-aluminum/FTO/glass (for devices with mask) or FTO/glass (for devices with no mask) substrates, allowing the formation of layers thick enough to prevent short circuit between the electrodes. After 30 min, the film was dry and presented very good quality. The aluminum top electrode was deposited by e-beam evaporation. The structures of the devices are presented in Fig. 1.

The FTO (500 nm)/glass substrates were cut in pieces of 15×10 mm^2 and arranged to leave areas of 2×1 mm^2 that became the devices bottom electrode, having connections with pads for electrical measurements. Onto them (in the case of mask devices), aluminum has been vacuum evaporated through a shadow mask forming an aluminum film covering the whole 2×1 mm^2 area of the FTO.

The holes in this aluminum/FTO/glass structure, hereafter called the mask film, were produced with the indentation technique.[18] The indentations were made using a nanoindenter XP (MTS Nanoinstruments) with a Berkovich indenter. The equipment performs the indentations by controlling the applied load with a resolution better than 1 μN. The displacement of the indenter tip into the surface are determined with resolution better than 1 nm. The Berkovich diamond tip has a triangular pyramidal shape of faces forming an angle of 65.3° with the vertical axis. The applied loads were between 20 and 100 mN.

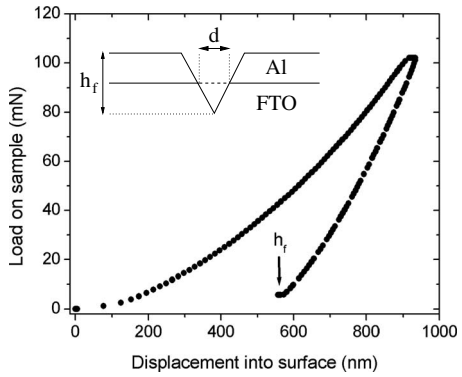

FIG. 2. A typical load vs displacement curve. Here for a 60 nm aluminum film in the mask and a maximum load of 100 mN. The inset shows a schematic transversal view of an indentation, producing a hole characterized by the depth h_f and the lateral size at the Al/FTO interface d.

For each device sample, a 20×8 matrix of indentation holes was made in the aluminum of the mask film. The atomic force microscopy (AFM) image of these indentations was generated in dynamic mode and with a silicon probe from a Shimadzu SPM 9500J3. The size and depth of the indentations were determined from such images. Also, images of the indentation matrices were obtained by optical microscopy. The devices with and without a mask were then electro-optically characterized through measurements of the photocurrent (at zero bias) versus the wavelengths of the incident light. The monochromatic light (of wavelengths between 300 and 800 nm) was generated by a tungsten halogen lamp from an Oriel MS257 monochromator. The photocurrents at zero bias were measured with a Keithley picoampmeter. Both equipments were connected to a homemade SICADI program data process system.

III. RESULTS AND DISCUSSION

The optimum wavelength for the P3HT:PCBM blend absorption is 550 nm.[19] Hence, we have performed a series of tests with the nanoindenter in order to produce holes of transversal size d at the aluminum/FTO interface (see inset of Fig. 2) of around 500 nm.[20] We have found that the appropriate maximum loads to be applied depend not trivially on the thickness of the aluminum in the mask. In fact, the influence of the substrate (FTO) is very important. Note that the hardness of the FTO is higher than that of aluminum. Thus, thinner films demand greater maximum loads than thicker aluminum films, a not so obvious result at first sight.

A typical load versus the displacement curve is shown in Fig. 2 (for a maximum load of 100 mN). From the graph, we can observe an elastic recovery during unloading. The indentation depth after unloading h_f (inset of Fig. 2) can be determined from the load-displacement data. However, more precise values are obtained directly from the AFM images of the indentation matrices, an example is displayed in Fig. 3. So, we have used the AFM cross section profile images to determine the holes dimensions.

Once the best maximum load for a given thickness have been determined, we fabricated the mask films by indenting the holes in a regular arrangement, a square lattice of lattice parameter s. We should observe that the used nanoidenter

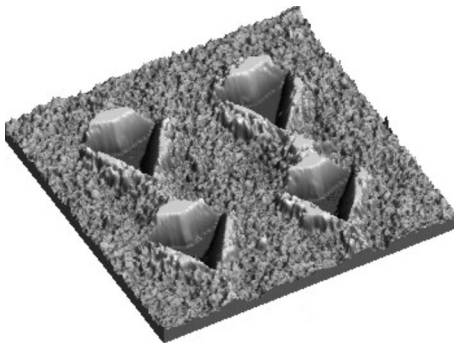

FIG. 3. AFM image of a squared matrix (30×30 μm^2) of nanoindented holes made in the aluminum film (320 nm)/FTO/glass mask. Applied maximum load of 100 mN and $s=7.5$ μm.

allowed a good control over the distance s between the holes. Figure 4 shows an indentation matrix with $160(20\times8)$ indentations, made for a maximum load of 100 mN and $s=25$ μm, then 50 times the hole transverse size $d=500$ nm.

A key aspect in our goal to trap the light within the device to improve light harvesting is to properly choose the values of s based on a compromise to get as much light as possible into the active polymer layer and, once there, to minimize the escape of photons from the region. Such type of strategy has been successfully used in Ref. 14 by means of a metallic film with a single aperture (hole) placed on top of the glass substrate. In the present contribution, the idea is that with an array of holes mask, we can drastically increase the availability of incident light. Indeed, it is known that under appropriate conditions, light transmission through a periodic structure of holes in a metallic film can be very high.[21–23] On the other hand, if the holes are not located too close together, we also can hinder an appreciable "leaked" from the system cavity. The sought situation is schematically represented in Fig. 5(a).

Therefore, we shall look for s leading to an adequate field distribution (i.e., reasonable intense and homogeneous) in the cavity. We observe that for so we do not need a very detailed and precise description of the field for each s, but only to determine *relatively* which s results in the optimal outcome. Thus, we can make some reasonable approximations that strongly reduce the calculations, avoiding the necessity of more complete and sophisticated, but more complicated, theoretical approaches like that developed in Ref. 23.

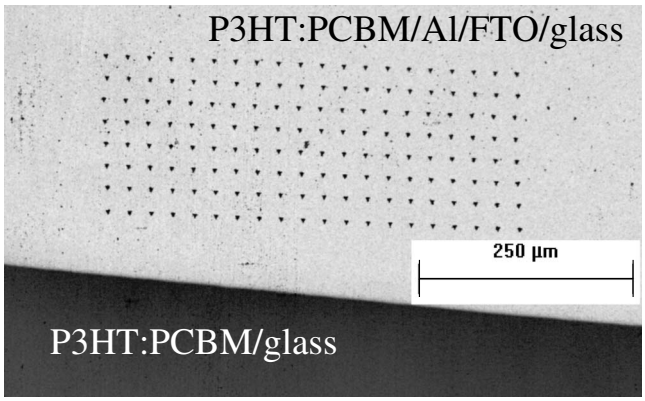

FIG. 4. An optical microscopy image of a device (before the top electrode deposition), showing in detail the indentation 20×8 matrix with $s=25$ μm.

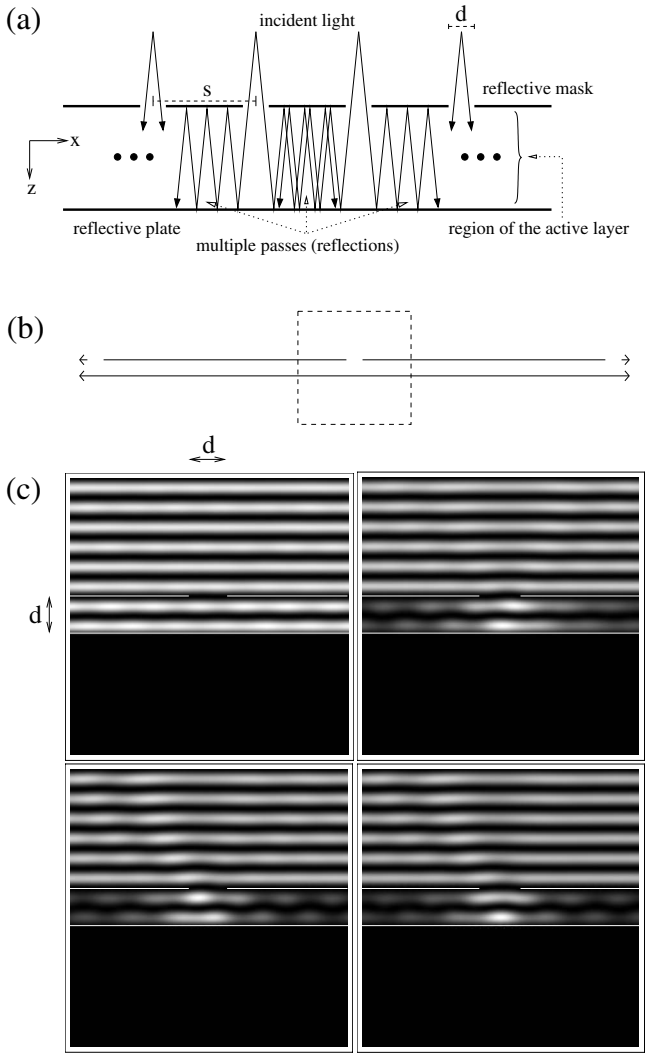

FIG. 5. (a) Schematic representation of the light behavior in the x-z plane section of the device. (c) Density plots of the simulated field distributions, in the region (around a mask hole) indicated in (b), for an incident plane wave of $\lambda=d=500$ nm. The panels represent anticlockwise (from top-left): $s=15\times d$, $s=40\times d$, $s=50\times d$, and $s=30\times d$.

In this way, as discussed in the Appendix, we can address an associated and much simpler two-dimensional (2D) scattering problem of a plane wave of wavelength λ propagating along the $+z$ direction, incident on the holes structure [depicted in Fig. 5(a)], and then forming a steady state pattern within the cavity. This scalar field $\Psi(x,z)$ obeys the Helmholtz equation $\nabla^2\Psi(x,z)+k^2\Psi(x,z)=0$ for $k=2\pi/\lambda$, and satisfies the Dirichlet boundary conditions both in the walls of the mask and in the reflective plate (in the device, the top aluminum electrode). It is easily treated by the so-called boundary wall method,[24] an approach already used to study, e.g., open resonators,[25] photonic crystals,[26] and quantum wires.[27] For a complete account of how to implement the method numerically, one can see Ref. 28.

In Fig. 5(c) we display, for some representative s (in units of d), the corresponding square of the field intensities

TABLE I. Parameters of the different device samples.

Sample	Al thickness (nm)	Load (mN)	Spacing between indentations s (μm)	Dimensions of the holes at the Al/FTO interface d (nm)	s/d
1	60	100	25	~500	50
2	60	100	50	~500	100
3	320	20	7.5	~500	15
4	320	20	20	~500	40
5	no mask	⋯	⋯	⋯	⋯

$|\Psi(x,z)|^2$ in the region indicated in Fig. 5(b). As the incident wavenumber we take $\lambda = d$. Since the active layer has a thickness of 500 nm in all the actually produced samples, we assume in the calculations that the distance between the reflective mask and plate [Fig. 5(a)] is also d. We clearly see that by varying s, one has different field distributions in the cavity. From many simulations, we have found that for our purposes, $s = 15\lambda$ is the best geometric configuration for the device mask. Hence, we should expect higher efficiencies in this case, which is exactly what we verify next.

To test the performance of the proposed devices, we have produced a total of five samples. One, for comparison, is the usual case without a mask and the others with masks of different s and aluminum film thicknesses. The systems parameter values are summarized in Table I. We should mention that all the samples have been fabricated in a similar way and with the same polymer thickness of 500 nm. Also, the results were reproducible.

For each device, we have measured the photocurrent density as a function of the incident monochromatic light wavelength λ. In Fig. 6(a) we show the curves for the plain (no mask) case and for the mask film devices with $s = 40 \times d$ (aluminum film thickness of 320 nm), $s = 50 \times d$ (aluminum film thickness of 60 nm), and $s = 100 \times d$ (and aluminum film thickness of 60 nm). For $\lambda > 400$ nm, we see that the device with $s = 50 \times d$ always presents the higher photocurrents. Moreover, if we consider only the most important interval for the polymer absorption $450 \leq \lambda \leq 700$ nm, the $s = 40 \times d$ sample is, in average, also better than the conventional device (just compare the areas under the curves in the mentioned wavelength range). On the other hand, for the $s = 100 \times d$ device the efficiency is much lower. Qualitatively, it is easy to understand from the fact that for such s value, large regions of the active layer are not illuminated and this is not compensated by eventual constructive interference enhancing the amount of light within the cavity nearby the holes locations.

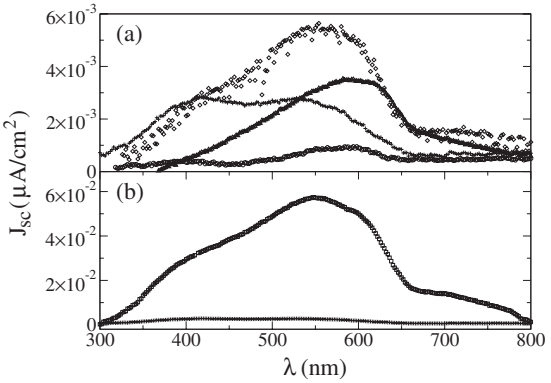

FIG. 6. The photocurrent density vs the incident light wavelength. All the devices have the same active layer thickness. (a) Devices with $s = 40 \times d = 20$ μm and a mask of a 320 nm thick aluminum film (triangle); $s = 50 \times d = 25$ μm and a mask of a 60 nm thick aluminum film (diamond); and $s = 100 \times d = 50$ μm and a mask of a 60 nm thick aluminum film (circle). (b) Device with $s = 15 \times d = 7.5$ μm and a mask of a 320 nm thick aluminum film (square). For comparison, in both plots the curve (+) represents the device without any mask.

In Fig. 6(b) we display the $J_{sc} \times \lambda$ curves for the plain device of Fig. 6(a) and for the device with $s = 15 \times d$ (and aluminum film thickness of 320 nm). The plot actually agrees with the theoretical prediction that for this particular s size the photocurrent is considerably increased by one order of magnitude for λ around the active layer optimal wavelength absorption (of 550 nm). So, a constructive interference generating a trapped and relatively well distributed field inside the device cavity (Fig. 5(c), top-left panel), in fact, greatly improves the system efficiency.

Regarding the observed behaviors in Fig. 6, three final comments are in order. (i) The sample with $s = 50 \times d$ is obviously better than that with $s = 40 \times d$. From a rapid inspection in the density plots of Fig. 5(c), it seems that these two cases have fairly similar field distributions within the device cavity. However, an accurate and detailed calculation of the field Ψ in the vicinity of the holes (what we have done, but do not show the numerics here) leads to the conclusion that for $s = 50 \times d$, the field is a little higher and more homogeneously distributed in these regions, thus explaining the efficiencies' difference. (ii) As it should be from the simulations— which we recall are based only on the variations in the parameters s and d—we find that the $s = 15 \times d$ device (fabricated with an aluminum film of 320 nm) has a better performance than that with $s = 50 \times d$ (fabricated with an aluminum film of 60 nm). It is worth noting, however, that both curves have very similar general shapes (indeed, see the corresponding graphs in Figs. 6(a) and 6(b)), even though the mask films have different thicknesses. By its turn, the sample with $s = 50 \times d$ is better than the one with $s = 40 \times d$ (fabricated with an aluminum film of 320 nm). So, all these results are an indication that the most important feature for the system efficiencies is the actual value of s (and of d), and not the exact thickness of the aluminum film used, at least in the range tested of 60–320 nm. (iii) Lastly, we have

performed simulations for $s < 10 \times d$, finding that some s values may also give good field distribution inside the cavity. Nevertheless, in such cases, very small variations in either s or d can completely destroy the constructive interference patterns. Thus, in principle, one can produce devices with enhanced performances for s smaller than $10 \times d$, but then the mask film fabrication procedure should be very well controlled.

IV. REMARKS AND CONCLUSION

In summary, to promote light trapping in organic photovoltaic devices, we have used metal mask films with indented holes of chosen size d and spacing s. For d, we have set a value close to the P3HT:PCBM maximum absorption wavelength. This has allowed relevant light diffraction (through the mask holes) exactly in the absorption spectrum interval of the system active layer. To investigate the influence of s on the field distribution inside the device cavity, we have considered a very simple model. Based on it, we have then fabricated devices with different holes spacing values, also characterizing their action spectra. In the cases where the simulations predicted a good field distribution, the corresponding $J_{sc} \times \lambda$ curves indeed have shown higher photocurrents than those for the traditional device (i.e., only with transparent electrode and no mask).

Our theoretical analysis focused on just the geometrical aspects of the device cavity, not taking into account the optical properties of the active layer filling the cavity. Thus, assuming only the empty device structure by means of straightforward and reasonable assumptions, we have drastically reduced the numerical work necessary to obtain the sought field patterns. In fact, we have not addressed the full set of three-dimensional Maxwell equations for the electromagnetic field, but instead we solved a 2D scalar Helmholtz equation in analogy to what is done for the TE modes calculations in certain optical structures (Appendix). Even with such simplifications, we have been able to find appropriate s values leading to enhanced efficiencies; in the best case, one order of magnitude higher than that of a usual device. Nevertheless, the use of more complete theoretical approaches,[22,23] including a correct description of light propagation and attenuation within the active layer,[2,29] to treat the filled device cavity certainly would "refine" the obtention of the optimal parameters values. It is a work in progress and the results will be reported in due course.

Regarding the possible effects of nanoindented electrodes on the device active layer charge transport features, we shall comment the following. The metal in the mask, aluminum, has a work function (~4.3 eV) which is close to that of the FTO (~4.4–4.8 eV). Therefore, the mask does not modify sensibly the injection. On the other hand, the holes could eventually influence the polymer morphology at the electrode/polymer interface (but only locally, since the total area of the holes is much smaller than the total area of the electrode). However, we have verified that the $J \times V$ curves at the dark, for devices with and without masks, are very similar, with a same magnitude for J. So, the holes modify the photocurrent but not the current in the dark. This is an indication that the masks with nanoindented holes have not importantly changed the transport properties in our systems.

Finally, we should observe the conductivity of the aluminum film with holes is higher than that of transparent oxides (FTO). In this way, eventually, an indented metal mask film (without the present expensive transparent electrode) itself could act as the electrode. Moreover, such a metal mask electrode could be deposited onto flexible substrates, thus being produced in roll to roll processes. This possibility is under investigation.

ACKNOWLEDGMENTS

We acknowledge research fellowships from CNPq and CAPES, and also grants from Finepe/CT-Infra, CNPq/CT-Energ, CNPq/Reman, CNPq/RENAMI, CNPq/Edital Universal, and Fundação Araucária.

APPENDIX

Here we argue *heuristically* why, to find s for appropriate field distributions within the device cavity, we can address a reduced scalar 2D scattering problem. We start observing that, since we have an incident monochromatic plane wave, we can suppose the temporal dependence $\exp[-i\omega t]$ ($\omega = kc$). Thus, the fields spatial part, say $\mathbf{E}(\mathbf{r})$ and $\mathbf{H}(\mathbf{r})$, are obtained from the set of time-independent Maxwell equations

$$\nabla \times \mathbf{E} = +i\omega\mu_0 \mathbf{H} \quad \nabla \cdot \mathbf{H} = 0,$$

$$\nabla \times \mathbf{H} = -i\omega\epsilon_0 \mathbf{D} \quad \nabla \cdot \mathbf{E} = 0. \tag{1}$$

We recall that for the simpler situation we are analyzing [Fig. 5(a)], the propagating dielectric media is always taken as air. Also, we do not consider a more detailed (microscopic) description of the holes.[22] We just face them as diffraction slits, assuming appropriate boundary conditions on the metal surfaces of the mask (likewise for the reflective plate, the top electrode).

From the system rectangular symmetry, a reasonable approximation is to assume that the fields are given by a certain pattern in the x-z plane, multiplied by an "envelope" in the y direction, which should present typical sinelike oscillations. With this picture in mind, we expect to obtain the (almost) ideal case by just focusing the optimization of the field distribution in the x-z plane. Possible changes in the ubiquitous oscillatory behavior along y (through variations in s) cannot improve the overall fields if the x-z profiles are far away from their best configurations. Indeed, observe that the system is fairly symmetric regarding the x and y directions. Hence, if a given s improves the distribution in the x-z plane (thus, somewhat along x), it probably is already close to the value leading to the most appropriate field profile along y.

So, for our purposes and under the above simplifying assumptions, we can just disregard the field y dependence in the Maxwell equations. In this case, Eq. (1) reduces[30] to independent scalar Helmholtz equations for both the electric and magnetic field intensities, a very common situation, e.g., in 2D photonic crystals.[31] Then, the resulting TE modes for the electrical field correspond to the y component $E_y(x,z)$,

for which $\nabla^2 E_y(x,z)+k^2 E_y(x,z)=0$ $(k=2\pi/\lambda)$ with the Dirichlet boundary conditions in the metallic walls. By identifying $\Psi(x,z)$ with $E_y(x,z)$, we end up exactly with the problem discussed in Sec. III.

[1] L. S. Roman, W. Mammo, L. A. A. Pettersson, M. R. Andresson, and O. Ingans, Adv. Math. **10**, 774 (1998); L. Chun Chen, O. Inganäs, L. S. Roman, M. Johansson, and M. R. Andersson, Thin Solid Films **363**, 286 (2000); S. E. Shaheen, C. J. Brabec, N. S. Sariciftci, F. Padinger, T. Fromherz, and J. C. Hummelen, Appl. Phys. Lett. **78**, 841 (2001); R. Valaski, C. D. Canestraro, L. Micaroni, R. M. Q. Mello, and L. S. Roman, Sol. Energy Mater. Sol. Cells **91**, 684 (2007).

[2] M. Koehler, L. S. Roman, O. Inganäs, and M. G. E. da Luz, J. Appl. Phys. **96**, 40 (2004).

[3] *Organic Photovoltaics: Mechanism, Materials, and Devices*, edited by S. S. Sun and N. S. Sariciftici (CRC, Boca Raton, FL, 2005).

[4] C. Arbour, N. R. Armstrong, R. Brina, G. Collins, J. Danziger, J.-P. Dodelet, P. Lee, K. W. Nebesny, J. Kankow, and S. Waite, Mol. Cryst. Liq. Cryst. **183**, 307 (1990); J. J. M. Halls, C. A. Walsh, N. C. Greenham, E. A. Marseglia, R. H. Friend, S. C. Moratti, and A. B. Holmes, Nature (London) **376**, 498 (1995).

[5] D. Cheyns, H. Gommans, M. Odijk, J. Poortmans, and P. Heremans, Sol. Energy Mater. Sol. Cells **91**, 399 (2007).

[6] M. Y. Chan, S. L. Lai, M. K. Fung, C. S. Lee, and S. T. Lee, Appl. Phys. Lett. **90**, 023504 (2007).

[7] C. Winder and N. S. Sariciftci, J. Math. Chem. **14**, 1077 (2004); A. K. Pandey, S. Dabos-Seignon, and J. M. Nunzi, Appl. Phys. Lett. **89**, 113506 (2006); S. Gunes, H. Neugebauer, N. S. Sariciftci, H. Roither, M. Kovalenko, G. Pillwein, and W. Heiss, Adv. Funct. Mater. **16**, 1095 (2006); T. Shiga, K. Takechi, and T. Motohiro, Sol. Energy Mater. Sol. Cells **90**, 1849 (2006).

[8] S. Fan, P. R. Villeneuve, and J. D. Joannopoulos, Phys. Rev. Lett. **78**, 3294 (1997); L. I. Halaoui, N. M. Abrams, and T. E. Mallouk, J. Phys. Chem. B **109**, 6334 (2005).

[9] C. F. Madigan, M. H. Lu, and J. C. Sturm, Appl. Phys. Lett. **76**, 1650 (2000).

[10] T. Tsutsui, M. Yahiro, H. Yokogawa, K. Kawano, and M. Yokoyama, Adv. Math. **13**, 1149 (2001).

[11] M. Agrawal, Y. Sun, S. R. Forrest, and P. Peumans, Appl. Phys. Lett. **90**, 241112 (2007).

[12] L. S. Roman, O. Inganäs, T. Granlund, T. Nyberg, M. Svesson, M. R. Andersson, and J. C. Hummelen, Adv. Math. **12**, 189 (2000).

[13] K. Tvingstedt, V. Anderson, F. Zhang, and O. Inganäs, Appl. Phys. Lett. **91**, 123514 (2007).

[14] P. Peumans, V. Bulovic, and S. R. Forrest, Appl. Phys. Lett. **76**, 2650 (2000).

[15] P. Peumans, V. Bulović, and S. R. Forrest, Appl. Phys. Lett. **76**, 3855 (2000).

[16] P. Peumans, A. Yakimov, and S. R. Forrest, J. Appl. Phys. **93**, 3693 (2003).

[17] J. C. Hummelen, B. W. Knght, F. Le Peg, F. Wuld, J. Yao, and C. L. Wilkins, J. Org. Chem. **60**, 532 (1995).

[18] C. M. Lepienski and C. E. Foerster, in *Encyclopedia of Nanoscience and Nanotechnology*, edited by H. S. Nalwa (American Scientific, Stevenson Ranch, CA, 2004), Vol. 7.

[19] S. Günes, H. Neugebauer, and N. S. Sariciftci, Chem. Rev. (Washington, D.C.) **107**, 1324 (2007).

[20] We should mention that we also have tested few devices with different d's, but the best outcomes for the photocurrents were always those with $d \approx 500$ nm. So, in the present work we report only the optimal case.

[21] T. W. Ebbesen, H. J. Lezec, H. F. Ghaemi, T. Thio, and P. A. Wolff, Nature (London) **391**, 667 (1998); H. F. Ghaemi, T. Thio, D. E. Grupp, T. W. Ebbesen, and H. J. Lezec, Phys. Rev. B **58**, 6779 (1998).

[22] W. L. Barnes, A. Dereux, and T. W. Ebbesen, Nature (London) **424**, 824 (2003).

[23] F. J. García de Abajo, R. G.-Medina, and J. J. Sáenz, Phys. Rev. E **72**, 016608 (2005).

[24] M. G. E. da Luz, A. S. Lupu-Sax, and E. J. Heller, Phys. Rev. E **56**, 2496 (1997).

[25] J. A. Katine, M. A. Eriksson, A. S. Adourian, R. M. Westervelt, J. D. Edwards, A. Lupu-Sax, E. J. Heller, K. L. Campman, and A. C. Grossard, Phys. Rev. Lett. **79**, 4806 (1997).

[26] P. V. Parimi, W. T. Lu, P. Vodo, J. Sokoloff, J. S. Derov, and S. Sridhar, Phys. Rev. Lett. **79**, 4806 (1997); F. M. Zanetti, M. L. Lyra, F. A. B. Fidelis, and M. G. E. da Luz (unpublished).

[27] J. Y. Vaishnav, A. Itsara, and E. J. Heller, Phys. Rev. B **73**, 115331 (2006); J. Y. Vaishnav, J. D. Wall, M. Apratim, and E. J. Heller, Phys. Rev. E **76**, 013620 (2007).

[28] F. M. Zanetti, E. Vicentini, and M. G. E. da Luz, Ann. Phys. (N.Y.) **323**, 1644 (2008).

[29] L. A. Pettersson, L. S. Roman, and O. Inganäs, J. Appl. Phys. **86**, 487 (1999).

[30] W. R. Frei and H. T. Johnson, Phys. Rev. B **70**, 165116 (2004); A. E. Miroshnichenko and Y. S. Kivshar, Opt. Express **13**, 3969 (2005).

[31] P. Kuchment, in *Mathematical Modeling in Optical Science*, edited by G. Bao, L. Cowsar, and W. Masters (SIAM, Philadelphia, 2001).